THE ASTRONOMICAL JOURNAL VOLUME 112, NUMBER 3 SEPTEMBER 1996

DIFFERENTIAL BINARY STAR PHOTOMETRY USING THE ADAPTIVE OPTICS SYSTEM AT STARFIRE OPTICAL RANGE

T. A. ten Brummelaar, B. D. Mason, W. G. Bagnuolo, Jr., W. I. Hartkopf, H. A. McAlister, and N. H. Turner

Center for High Angular Resolution Astronomy, Georgia State University, Atlanta, Georgia 30303
Electronic mail: theo,mason,bagnuolo,hartkopf,hal,nils@chara.gsu.edu

Received 1996 May 16; revised 1996 June 18

ABSTRACT

As part of an NSF effort to make the Starfire Optical Range 1.5-m telescope, equipped with laser guide star and adaptive optics, available to the astronomical community, several nights in 1995 May and October were awarded to the CHARA group in order to perform differential photometry on close binary stars. Images were acquired in two near-IR pass bands of over twenty pairs and reduced by fitting both the point spread function (PSF) and the positions and intensities of the stars. The Δm values were calibrated using ten stars for which combined I and R photometric data were available in the literature. Color indices have been calculated for the individual components of these stars, allowing for the determination of spectral classifications of both components in seven of the systems.

1. INTRODUCTION

The only fundamental source for many of the basic properties of stars is through the analysis of binary stars. For over twenty years, astronomers within Georgia State University's Center for High Angular Resolution Astronomy (CHARA) have conducted binary star research using the method of speckle interferometry at the largest ground-based telescopes available. While speckle provides diffraction-limited resolution and has been highly successful in determining the astrometry of binary stars and deriving orbital properties (e.g., Hartkopf *et al.* 1996a), the determination of magnitude difference has been an elusive goal. Only through the direct measurement of Δm can we place the individual components of a binary star system on an empirical mass/luminosity plot. Furthermore, measurement of Δm at two or more wavelengths ties the masses and luminosities to an effective temperature.

Despite its fundamental importance, there are very few Δm measurements for astrophysically significant binaries. This is not through a lack of effort. Visual double star observers often estimate magnitude difference as they measure the astrometry of binary star systems (see, for example, the *Washington Double Star Catalog*, maintained at the USNO). The use of objective gratings to determine magnitude differences was pioneered by Kuiper (1935a, 1935b), and later used by Lindenblad (1970) to determine the Δm of the Sirius AB system. Birefringent prism micrometery by Pickering (1879) and Muller (1948, 1949) allowed for Δm determinations as well, sometimes for systems as close as 0.″5. Area scanner observations by Franz (1970) have estimated Δm for wider systems. More conventionally, photographic estimates of Δm for wide pairs were standardized by Strand (1969). Many of the results from these complimentary techniques were collected in the catalog of Wierzbinski (1969) and the more recent *Catalog of Photometric Magnitude Differences* (maintained at the USNO). Recent efforts have used CCDs to obtain the photometry of individual components (for example, Tokovinin & Shatskii 1995). Here again, however, the systems which are measured are typically wide.

Lunar occultation provides measurements of the Δm of binaries. However, the events are restricted to zodiacal band stars and are infrequent and unrepeatable occurrences. Also, the Δm determinations from lunar occultation have suffered from large errors and were often taken with non-standard filters (Mason 1994, 1995).

For speckle data analysis, the ''fork'' algorithm (Bagnuolo & Sowell 1988) is only applicable to a photon-noise-limited detector with more than 5 photons per speckle, while the ''directed vector-autocorrelation'' has errors which are too large without laborious calibrations (which in turn, decreases observational efficiency by as much as a factor of 40; Mason *et al.* 1993). Full image reconstruction from non-redundant aperture masking is possible, and work on this at CHARA continues (Roberts *et al.* 1996).

Alternatively, near diffraction-limited images can be obtained using adaptive optics. Presented here are preliminary results from an adaptive optics observing run in 1995 October using the Starfire Optical Range 1.5-m telescope (Fugate *et al.* 1994) located on Kirtland Air Force Base near Albuquerque, New Mexico. The SOR facility is equipped with an adaptive optics (AO) system and laser guide star. The goal of this observing run was to determine accurate magnitude differences in more than one bandpass from a sample of close visual binary stars for the purpose of spectral classification and effective temperature estimation.

2. DATA COLLECTION

Two observing runs were awarded to the CHARA group, one in May and the other in 1995 October. During the May run we attempted to obtain images with the longest

 0004-6256/96/112(3)/1180/8/$10.00

possible integration times, in order to obtain high signal-to-noise data. Unfortunately the AO system was not always stable for an entire integration, resulting in poor image quality. For the October run the methodology of data collection was changed. Many short-exposure images were collected for each target, and the best of these were summed together using a shift-and-add algorithm. It was also sometimes necessary to open the AO servo loop, re-acquire the object and close the servo loop again to achieve satisfactory results.

A second problem encountered was due to the varying performance of the laser guide star with zenith distance (ZD). The guide star created is not a point source, and therefore a 'laser reference' is required for laser operation. A laser reference is made by closing the AO servo on a bright natural star and propagating the laser at the same time. In this way the average shape of the reference spot created by the laser can be measured, which then becomes the reference shape used when closing the loop with the laser guide star. The shape of this spot varies with ZD, and new laser references are required whenever there is a substantial change. To maximize efficiency, observations were made at or near the same ZD for as long as possible. Otherwise a new laser reference was made. A subset of the CHARA speckle observing list was prepared so that suitable targets could be chosen at the current ZD whenever possible.

The data collection scheme was to observe a known single star (Hartkopf *et al.* 1996b) of similar brightness, color, and ZD to the binary. In this way we obtained an estimate of the point-spread function (PSF). This single star image also proved useful as an indication of the AO system performance. Indeed, some single stars appeared as doubles, due to errors in the AO system wavefront reconstructor. Multiple short exposures of the binary were then taken and stored, followed by another set of observations of the calibration star.

All observations were obtained with two different filters having central wavelengths and FWHM of 798 ± 108 and 884 ± 122 nm, respectively (Drummond 1995). These filters are hereafter designated 'r' and 'i.'

3. DATA REDUCTION

Two methods have been investigated for the reduction of the images: CLEAN (Roberts *et al.*, 1987) and an iterative PSF fit. In order for CLEAN (or any similar deconvolution algorithm) to work, one must have a good estimate of the current PSF. Usually this is provided by observing point sources and assuming enough instrumental stability for these images to be a good approximation to the PSF. During times of good seeing and when the source is bright enough to be used as a guiding object this works quite well. Figure 1 is an example of an image created using CLEAN. During tests CLEAN worked well up to an inflection point. In practice, however, the CLEAN algorithm fails if the two stars are not clearly separated in the raw image or if the PSF estimate is not good enough.

The alternative method is less general but, since the PSF is not always stable with an AO system, more reliable. Since we know that there are a finite number of stars in each frame,

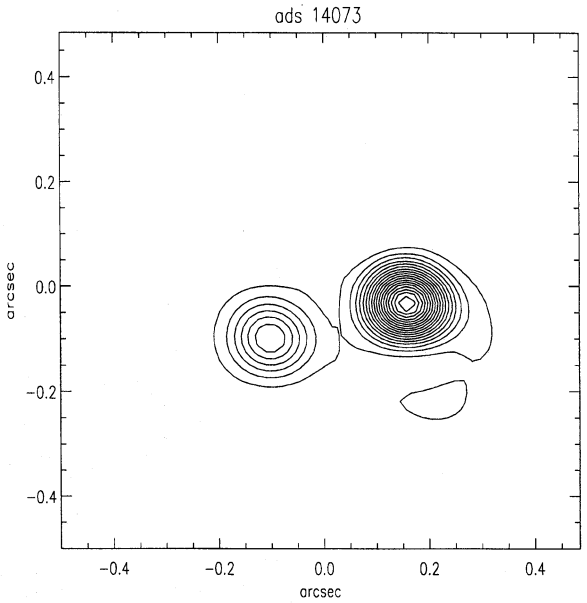

FIG. 1. An image reconstruction by the CLEAN algorithm of the binary star ADS 14073 in the i filter from an estimated PSF provided by the single star HR 8173. The estimated CLEANed image was reconvolved by an Airy function representing the aperture diffraction-limit. A loop gain of 0.2 was used for 450 iterations. The estimated intensity ratio was 0.365, as compared to 0.397 from the parameter-fitting method outlined in the text. The contour lines shown are at 5% levels.

we know the final 'image' should simply contain a number of delta functions. Thus, if there are known to be N stars in the field, the 'true' image should be given by

$$I(x,y)=\sum_{i=1}^{N} A_i\delta(x-x_i,y-y_i), \tag{1}$$

where A_i is the intensity of object i, (x_i,y_i) is the position of the object and

$$\delta(x,y)=\begin{cases}1 & \text{for } x=0 \text{ and } y=0\\ 0 & \text{otherwise.}\end{cases} \tag{2}$$

The observed image is then given by the convolution of the PSF, $P(x,y)$, and the true image

$$O(x,y)=I(x,y)*P(x,y). \tag{3}$$

This assumes that the PSF is constant throughout the field of view of the image. This is not a good assumption for large fields of view but works well for the small 2×2 arcsecond fields used for these data.

In order to obtain good first estimates for the positions and intensities of the stars, the image is inspected and the positions of the stars are entered manually. An image of a single star is used as the first estimate for the PSF. The fitting process is then a second order iterative method:

(1) Using the current delta functions, deconvolve the PSF from the image.

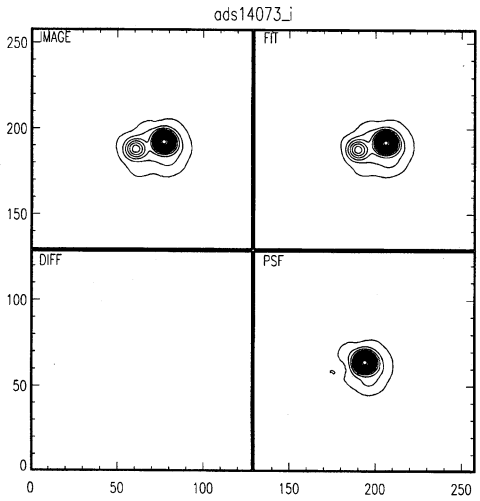

FIG. 2. The raw image (upper left), fitted image (upper right), difference (bottom left) and PSF (bottom right) for the star ADS 14073 in the *i* filter. The contour lines are at 5% levels scaled to the image minimum and maximum. The PSF maximum intensity has been increased to that of the image so some detail can be seen. The rms residual error was 0.02% of the image maximum intensity and the maximum residual error was 2.4%.

(2) Using the new PSF, use a non-linear least squares fit to find new values for A_i, x_i and y_i.
(3) Repeat steps 1 and 2 until the rms error changes by less than 1%.

The deconvolution can be done in Fourier space by dividing the Fourier transform of $O(x,y)$ by the transform of $I(x,y)$ and calculating the inverse transform of the result. However, the division can cause numerical problems when the magnitudes in the complex plane are very small. An alternative method is to use the current PSF and perform subtractions in the image plane. For example, an estimator of the PSF based on star i is

$$P_i(x,y)=O(x,y)-\sum_{j\neq i} A_j(\delta(x-x_j,y-y_j)*P_{\text{old}}(x,y)). \quad (4)$$

This can be done for each star in the field and a new PSF estimate created by forming a weighted average of these PSF estimators

$$P_{\text{new}}(x,y)=\frac{1}{\sum_{i=1}^{N}A_i}\times\sum_{i=1}^{N} A_iP_i(x,y). \quad (5)$$

If the current values for the position and size of the stars in the frame are not correct the deconvolved PSF will contain some energy from all the stars, resulting in a PSF consisting of a large central peak with smaller peaks around it in the relative positions of the other stars. Since the early estimates for the star positions and intensities are not exact, this leaking of energy from the fainter stars to the primary is inevitable, causing the PSF itself to become a binary. While the rms residual of the fit is not affected by this phenomenon the intensity ratios are affected, resulting in an incorrect Δm measurement. In order to avoid this problem a mask was

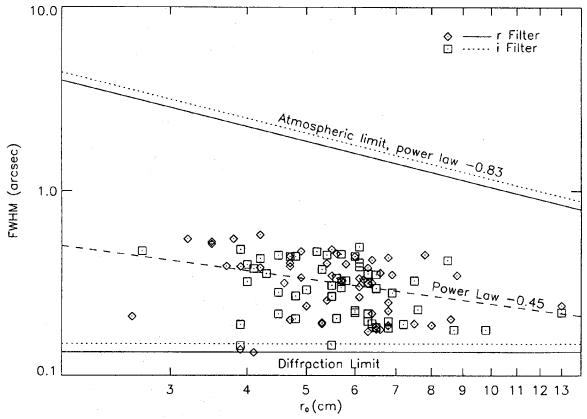

FIG. 3. The full-width-half-maximum measured while using the AO system for all of the stars observed during the run plotted against the current r_0.

made for each object based on the single star image. This mask is set to one in the area of the single star where the intensity is significantly greater than zero and has a Gaussian roll-off to zero beyond this area. Every time a new PSF estimate is made it is multiplied by this mask and then normalized so that

$$\int P(x,y)dx\,dy=1.0. \quad (6)$$

One then iterates Eqs. (4), (5) and (6) until the rms residual error of the fit changes by less than 1%. An example of the raw image, fit, difference and PSF is shown in Fig. 2 for the same observation as the CLEANed image of Fig 1.

4. IMAGE SCALE CALIBRATION

During the week preceding the run at SOR some of the potential binary targets were observed with the 100-inch Hooker telescope on Mount Wilson using the CHARA speckle camera. These data were reduced yielding separations and angular positions. Furthermore, a number of the binary systems in the SOR list have well-known orbits previously calculated by the CHARA group. The PSF fitting technique was used to calibrate the pixel scale of the images, leaving the separation as a free parameter. The resulting separations were fitted to a straight line resulting in the spatial scales of 64.3 ± 0.2 pixels per arcsecond in the i band and 63.4 ± 0.2 pixels per arc second in the r band. The focal planes for the two wavelengths were different, resulting in the small difference in image scales.

With the image scale calibrated it is possible to investigate the overall performance of the AO system. Shown in Fig. 3 is a plot of the full-width-half-maximum found for all the stars observed over the four nights, plotted against the r_0 provided by the SOR staff for the time of each observation. At the top are lines representing the equivalent atmospheric FWHM based on the r_0 for each filter, while below are two lines representing the diffraction limit of the optical system for each filter.

Clearly, one does not always obtain diffraction-limited

TABLE 1. Filter data.

Filter	Johnson (nm)	SOR (nm)
R/*r*	700±22	798±108
I/*i*	900±24	884±122

images, necessitating the use of the deconvolution algorithms described above. All of the images lie between the atmospheric and diffraction limits, with a fitted power law of −0.45, coincidentally nearly half that of the atmospheric power law of −0.83, although it is doubtful whether this has any physical meaning.

5. PHOTOMETRY

Combining the known binary position and the image pixel scale, the deconvolutions were repeated with the binary separations fixed but leaving the PSF and intensities of the stars as free parameters. Astrometric values were calculated from the orbits of Docobo & Costa (1990), Baize (1958, 1969, 1979), Dombrowski (1990), Hartkopf *et al.* (1989), extrapolation of published speckle measures (Hartkopf *et al.* 1996b) for ADS 15758 and a new calculation for ADS 4617. For ADS 4617, there were seen to be differences between the expected position based on the orbit of Heintz (1989) and the separation seen in the SOR data. Following the precepts of van den Bos (1962), no new orbit will be published at this time; however, this system may be ripe for a combined solution soon.

Because the wavelength of the laser guide star falls within the *V* band it was only possible to observe in the *i* and *r* bands at SOR. As described above, filters available at SOR were not standard Johnson filters (Allen 1973) as set out in Table 1. Furthermore the observation nights were not photometric. Nevertheless, it was found possible to calibrate the photometric scale well enough to obtain differential photometry of some binary systems.

A calibration equation of the form (Henden & Kaitchuck 1982)

$$m_R = m_r - k'_R X + \xi_{R1}(m_r - m_i) + \xi_{R2} \tag{7}$$

was used, where

$$m_r = -2.5 \log(A_{r1} + A_{r2}), \tag{8}$$

m_R is the combined magnitude in the *R* band, A_{r1} and A_{r2} are the intensities calculated during the PSF fitting process in the *r* band, and *X* is the airmass, which for the small ZD used is given by

$$X = \sec(\mathrm{ZD}). \tag{9}$$

The parameters k'_R, ξ_{R1} and ξ_{R2} are found by fitting Eq. (7) to the combined photometric data found in the literature (Lanz 1986). Note that the *R* and *I* magnitudes were calculated using tabulated *V*, *V*−*R* and *V*−*I* values and they therefore contain offsets due to the normalization of the color indices. Since this offset will only affect the ξ parameters

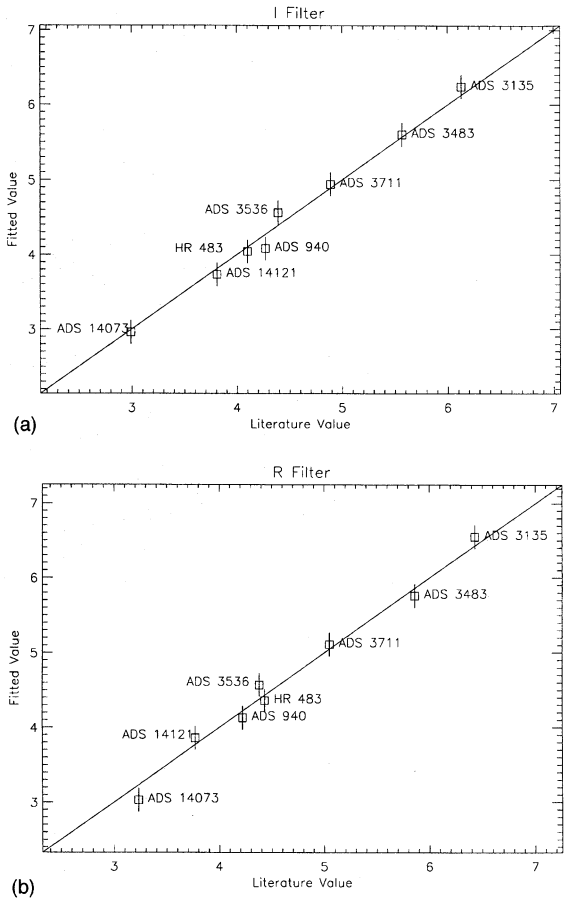

FIG. 4. Plot of the photometry calibration for both filters using the data from the first three nights. Part (a) shows the *i* filter data while (b) shows the *r* filter data.

(which we did not use in differential photometry), it is not critical to the rest of the data reduction. If one were interested in doing absolute photometry of these objects, these offsets would have to be taken into account. Analysis of the remaining double-star observations from the May and October SOR observing runs will be completed following *RI* photometry at GSU's Hard Labor Creek Observatory.

The parameters ξ_{R1} and ξ_{R2} were fitted across all observation nights while a different extinction parameter k'_R was used for each night. With this calibration, differential magnitudes can be found for each of the pairs using

$$\Delta R = \Delta m_r + \xi_{R1}(\Delta m_r - \Delta m_i). \tag{10}$$

Note that the differential magnitude only depends on the ξ_{R1} parameter. While these data are not sufficient for directly obtaining individual magnitudes, by combining the magnitudes from the literature and the differential magnitudes via

$$m_A = m + 2.5 \log(1 + 10^{-0.4\Delta m}), \tag{11}$$

it is possible to calculate the magnitudes of the individual components. Once again we note that there will be an offset in these magnitudes due to the color index normalization;

TABLE 2. Photometric calibration parameters.

Filter	rms residual	ξ_1	ξ_2	$k'_{\text{day 1}}$	$k'_{\text{day 2}}$	$k'_{\text{day 3}}$
R	0.13	0.61±0.29	30.4±1.7	13.2±1.7	13.2±1.6	14.1±2.0
I	0.11	1.12±0.24	26.6±1.4	9.1±1.6	9.1±1.6	9.9±1.6

however, since we are ultimately interested in calculating the $R-I$ values this is not important. A similar equation and parameter set were used for the I filter data.

When Eq. (7) was fitted to the data across all four nights of the October run, rms residuals of 0.15 mag for the R filter data and 0.13 mag for the I filter data were obtained. The fourth night, however, was intermittently cloudy, and the fit was recalculated using only the data for the first three nights. This resulted in rms residual errors of 0.13 and 0.11 mag for the R and I bands and it is this fit that has been used for the remainder of the Δm calculations. Figure 4 shows the resulting calibration curves for both filters while Table 2 contains the values of the fitted parameters. The differential photometry results derived using this calibration scale are given in Table 3.

6. ANALYSIS

A number of methods for allocating effective temperatures to the component stars were tried, all of which were based on the Kurucz (1994) photometric tables. A $\log(g)$ was selected appropriate for each star in question, with no reddening. In all cases splines were used to interpolate between the table values. In addition to the ΔR and ΔI data obtained from this run at SOR, ΔV measurements were located in the literature (Baize 1950, Dombrowski 1990, Muller 1949; Wickes 1975; Worley 1969), most were provided by the *Catalog of Photometric Magnitude Differences* (maintained at the USNO).

Since none of the observing nights were photometric and the filters available were not standard, it is likely that the differential photometric measurements, that is the ΔR and ΔI results, are the most reliable. Given these data, the χ^2 of a fit using the temperatures $T_{\text{eff},A}$ and $T_{\text{eff},B}$ is defined as

$$\chi^2(T_{\text{eff},A},T_{\text{eff},B}) = \frac{(\Delta V - V(T_{\text{eff},B}) + V(T_{\text{eff},A}))^2}{\sigma^2_{\Delta V}} + \frac{(\Delta R - R(T_{\text{eff},B}) + R(T_{\text{eff},A}))^2}{\sigma^2_{\Delta R}} + \frac{(\Delta I - I(T_{\text{eff},B}) + I(T_{\text{eff},A}))^2}{\sigma^2_{\Delta I}}, \quad (12)$$

where $\sigma^2_{\Delta V}$, $\sigma^2_{\Delta R}$, and $\sigma^2_{\Delta I}$ are the variances of the differential magnitude measurements. If both $T_{\text{eff},A}$ and $T_{\text{eff},B}$ were free parameters it was found that the χ^2 minimization was extremely unstable. During tests, if the "first guess" temperatures were very close to the "correct" answers, all these techniques converged quickly. If the first guess parameters were as much as 1% different from the correct answers, however, the fitting process either failed completely, moving to higher and higher temperatures for both components, converged on identical temperatures or temperatures too high to be reasonable. If a $T_{\text{eff},A}$ was fixed to a "known" temperature the process was stable.

Thus, even though the R-I measurements have larger formal errors they have been used in most cases to type the primary component. For small Δm systems, the color index has also been used for the secondary. A variation of these methods is to employ the literature value for the spectral type of the primary to get $T_{\text{eff},A}$ and then use the χ^2 minimization to find $T_{\text{eff},B}$.

The results of these processes are given in Table 4. Literature T_{eff} values were determined from the tables of Lang (1992) and the spectral types from the *Bright Star Catalogue* (Hoffleit & Warren 1992). Five results are shown for $T_{\text{eff},B}$. The first is based on the (R-I) measurement for the star with the error range representing the formal error of the estimate. The errors are large for the hotter stars due to the large slope of the (R-I) vs T_{eff} curve. The second estimate uses the $T_{\text{eff},A}$ found using our (R-I) results and the χ^2 mini-

TABLE 3. Photometric results.

Name	$(R-I)_{\text{lit}}$	ΔR	ΔI	$(R-I)_A$	$(R-I)_B$
ADS 755	0.500±0.028	0.503±0.021	0.508±0.009	0.502±0.036	0.497±0.043
ADS 940	−0.050±0.028	1.262±0.016	1.176±0.008	−0.071±0.033	0.015±0.038
ADS 3135	0.300±0.028	1.102±0.039	1.165±0.018	0.317±0.052	0.254±0.067
ADS 3483	0.290±0.028	1.398±0.031	1.443±0.015	0.300±0.045	0.254±0.056
ADS 3536	−0.010±0.028	1.075±0.018	0.859±0.009	−0.073±0.035	0.143±0.040
ADS 3711	0.160±0.028	0.719±0.048	0.976±0.015	0.240±0.058	−0.016±0.076
ADS 4617	0.090±0.028	1.746±0.055	1.309±0.021	0.004±0.065	0.440±0.088
ADS 14073	0.240±0.028	1.037±0.009	1.043±0.005	0.241±0.030	0.235±0.032
ADS 14121	−0.040±0.028	1.653±0.014	1.906±0.008	0.001±0.032	−0.252±0.036
ADS 15758	0.740±0.028	2.974±0.025	2.244±0.008	0.679±0.038	1.409±0.047

TABLE 4. Effective temperatures.

	$T_{eff,A}$	$T_{eff,B}$				
	Based on	Based on	Based on our $T_{eff,A}$ plus		Based on Literature $T_{eff,A}$ plus	
	$(R-1)_A$	$(R-I)_B$	$\Delta V,\Delta R\&\Delta I$	$\Delta R\&\Delta I$	$\Delta V,\Delta R\&\Delta I$	$\Delta R\&\Delta I$
ADS 755	4728± 155	4750± 224	4330±120	4320±120	4430±395	4420±390
ADS 940	12438±2063	9045± 864	7500±690	7460±690	7650±125	7620±125
ADS 3135	5887± 419	6429± 598	4600±240	4590±240	4720±170	4720±170
ADS 3483	6026± 388	6429± 500	—	4440±190	—	4650±195
ADS 3536	12550±1750	7403± 278	—	8220±730	—	6810±230
ADS 3711	6546± 537	9938±2375	5270±345	5200±335	6880±230	6730±220
ADS 4617	9312±2031	5052± 512	6110±800	6060±790	5970±120	5930±115
ADS 14073	6518± 268	6571± 286	5070±160	5060±160	5030±240	5020±240
ADS 14121	9406±1000	>40000	—	5360±285	—	5710±795
ADS 15758	4126± 90	<3500	—	<3500	—	<3500

mization process using the ΔV, ΔR and ΔI values while the third estimate does not include the ΔV data. The fourth and fifth estimates are similar except they use the $T_{eff,A}$ value based on the literature spectral classification.

The spectral classifications allocated to the stars based on these results are given in Table 5.

6.1 ADS 755

The magnitude difference in this system is small, so the literature spectral type will not necessarily be the same as that of the *A* component. The $T_{eff,A}$ based on the measured $(R\text{-}I)_A$ is consistent with a K3 V star. The $T_{eff,B}$ based on the measured $(R\text{-}I)_B$ has a large formal error, but also fits a K3 V best. Using the $T_{eff,A}$ based on $(R\text{-}I)_A$ and the ΔV, ΔR and ΔI measurements, yields a $T_{eff,B}$ consistent with spectral type K5 and with a much smaller formal error.

6.2 ADS 940

Based on the $R\text{-}I$ measurements the value of $T_{eff,A}$ is consistent with a B7 V star while $T_{eff,B}$ fits A2 V best. $T_{eff,B}$ based on the Δm's match a type of A8. Edwards (1976) determined spectral types of B6 IV and B9 V, which are not consistent with the observed colors and Δms.

TABLE 5. Spectral Classification

Name	Literature Classification	Assigned Types	
		A	*B*
ADS 755	K1IV	K3V	K5V
ADS 940	B7Ve	B7V	A8V
ADS 3135	F9V	F9V	K3V
ADS 3483	F5	—	—
ADS 3536	A1V	A1V	F1V
ADS 3711	A1V	A1V	F2V
ADS 4617	A2V	—	—
ADS 14073	F5IV	F5III	F3IV
ADS 14121	B9IV	A0V	G9V
ADS 15758	K2.5III	K3III	—

6.3 ADS 3135

This Hyades binary is the faintest star on the list. The fit is poor and noisy, which will affect $R-I$ and T_{eff} more than the Δm determination. Taking the literature spectral type for *A* of F9 V, the Δm's imply a K3 secondary.

6.4 ADS 3483

This multiple system is another Hyades object. The *A* component is a close pair classified as F5 V and G8 V while the *B* component is a G4 V (Turner *et al.* 1986). The Δm values are not consistent with this but rather imply a spectral type of K3 for the *B* component.

6.5 ADS 3536

The T_{eff} calculation is extremely sensitive to small errors for hot stars. While $T_{eff,A}$ based on the $(R-I)_A$ measurement is best fit by B7 V it has a large formal error, so the *A* component will be classified as an A1 V, consistent with the classification found in the *Bright Star Catalogue* (Hoffleit & Warren 1992). The $T_{eff,B}$ based on the $(R-I)_B$ measurement fits A9 V best, while the Δm's match an F2 V. The *B* component will therefore be taken as F1 V. This system is complicated by the *A* component being a 3.88-day spectroscopic binary (Lucy & Sweeney 1971); however, no contribution of the *Aa,b* component is seen in the spectrum (Harper 1911).

6.6 ADS 3711

The fit to the data here is quite poor and the formal errors are large, so only the Δm's are considered reliable. If we take the *A* component to be an A1 V, the ΔV, ΔI and ΔR values best match an F2 V type for the secondary.

6.7 ADS 4617

Edwards (1976) has previously classified this as A1 V +F2 V while Christy & Walker (1969) classified them as A2 V+F3 V. However, Fekel (1992, 1980) found this to be a quadruple system. The B component is a pair of F7V stars, and the A component an A8m plus a K or G dwarf. A more detailed analysis of this very complex system is not justified by the quality of these data, but the results are not inconsis-

tent with the results of Fekel (1992, 1980). Despite carrying a van Bueren number, this star is not believed to be a member of the Hyades cluster (Giclas *et al.* 1962) and was not included in the speckle survey of Mason *et al.* (1993).

6.8 ADS 14073

Christy & Walker (1969) classified this system as F6 III +F6 IV, while both Edwards (1976) and Gatewood *et al.* (1989) classified it as F5 III+F5 IV. $T_{\mathrm{eff},A}$ based on the $(R-I)_A$ measurement is consistent with F5 III, while the $T_{\mathrm{eff},B}$ based on the $(R-I)_B$ measurement fits F3 IV best. This is a speckle interferometry standard star (McAlister & Hartkopf 1983). Given the orbit of Hartkopf *et al.* (1989) and the parallax of $0''.0335 \pm 0''.0015$ determined by van Altena *et al.* (1991), the mass sum for the system is 3.36 ± 0.45 $\mathcal{M}_\odot$. Given the mass function of Abt & Levy (1976) and the calculated inclination, the individual components are most favored by a larger mass sum (from a smaller parallax). However, given the values at hand, we determine $\mathcal{M}_A = 1.68 \pm 0.33 \mathcal{M}_\odot$ and $\mathcal{M}_B = 1.68 \pm 0.17 \mathcal{M}_\odot$. While the smaller parallax fits better, there is also significant room for improvement of the spectroscopic elements over those presented in Abt & Levy (1976).

6.9 ADS 14121

$T_{\mathrm{eff},A}$ based on the $(R-I)_A$ measurement is consistent with A0 V (with an error of about 3 subclasses). The $(R-I)_B$ measurement implies a temperature >40,000 K so must be in error, however the Δm's imply a type G9 V.

6.10 ADS 15758

$T_{\mathrm{eff},A}$ based on the $(R-I)_A$ measurement fits a K3 III best. Because the magnitude differences are large in both bands, the $(R-I)_B$ measurement is not reliable. Indeed, all the methods for estimating $T_{\mathrm{eff},B}$ produced results less than 3500 K so are most likely in error.

7. CONCLUSION

Due to the lack of sufficient observations of photometric standard objects and the non-standard nature of the filters available, only differential photometry could be attempted on this data set. Nevertheless, the great potential of AO in the photometry of binary systems has been demonstrated, and effective temperatures and spectral types were found for the secondaries of seven systems.

If more time became available at SOR we would investigate the possibility of using standard *UBV* and/or *I* and *R* filters. This would allow better spectral classification of the components of many more multiple star systems. When newer AO systems specifically designed for astronomy come on line it will be possible to combine AO photometry with astrometry based on speckle interferometry and increase the dynamic range and signal-to-noise ratio of the method.

The authors would like to thank Robert Fugate, Earl Spillar, Julian Christou and all of the staff at Starfire Optical Range for their extensive efforts on our behalf. We gratefully acknowledge Charles Worley and Geoff Douglass of the US Naval Observatory for the use of the unpublished Catalog of Photometric Magnitude Differences and the Washington Double Star Catalog. This work was supported by the Center for High Angular Resolution Astronomy at Georgia State University through NSF Grant AST94-21259.

REFERENCES

Abt, H.A., & Levy, S.G. 1976, ApJS, 30, 273
Allen, C.W. 1973, Astrophysical Quantities, 3rd ed. (Athlone Press, London)
Altena, W.F. van, Lee, J.T.-l., & Hoffleit, E.D. 1991, The General Catalogue of Trigonometric Stellar Parallaxes (Yale University Observatory, New Haven)
Bagnuolo Jr., W.G., & Sowell, J.R. 1988, AJ, 96, 1056
Baize, P. 1950, J. Obs., 33, 1
Baize, P. 1958, J. Obs., 41, 165
Baize, P. 1969, Circ. Inf. No. 48
Baize, P. 1979, Circ. Inf. No. 79
Bos, W.H. van den, 1962, PASP, 74, 297
Christy, J.W., & Walker, R.L., Jr. 1969, PASP, 81, 643
Docobo, J.A., & Costa, J.M. 1990, PASP 102, 1400
Dombrowski, E.G. 1990, Ph.D. dissertation, Georgia State University
Drummond, J. 1995 (private communication)
Edwards, T.W. 1976, AJ, 81, 245
Fekel, F.C. 1980, PASP, 92, 785
Fekel, F.C. 1992, in Complimentary Approaches to Double and Multiple Star Research, IAU Colloquium 135, ASP Conf. Ser. Vol. 32, edited by H.A. McAlister and W.I. Hartkopf (ASP, San Francisco), p. 89
Franz, O.G. 1970, Lowell Obs. Bull., 17, 191
Fugate, R.Q., *et al.* 1994, JOSA, 11, 310
Gatewood, G., Castelaz, M., Persinger, T., Stein, J. Demarque, P., Sofia, S., & Stephenson, B. 1989, ApJ, 342, 1085
Giclas, H.L., Burnham, Jr., R., & Thomas, N.G. 1962, Lowell Obs. Bull., 5, 257
Harper, W.E. 1911, JRASC, 5, 115
Hartkopf, W.I., Mason, B.D., & McAlister, H.A. 1996a, AJ, 111, 370
Hartkopf, W.I., McAlister, H.A., & Franz, O.G. 1989, AJ, 98, 1014
Hartkopf, W.I., McAlister, H.A., & Mason, B.D. 1996b, Third Catalogue of Interferometric Measurements of Binary Stars, http://www.chara.gsu.edu/DoubleStars/Catalogues/Speckle/intro.html
Heintz, W.D. 1989, PASP, 101, 510
Henden, A.R., & Kaitchuck R.H. 1982, Astronomical Photometry (Van Nostrand Reinhold Company, New York)
Hoffleit, D., & Warren, Jr., W.H. 1992, The Bright Star Catalogue, 5th revised ed. (preliminary version)
Kuiper, G.P. 1935a, PASP, 47, 15
Kuiper, G.P. 1935b, PASP, 47, 121
Kurucz, R.L. 1994, Solar Abundance Model Atmospheres for 0,1,2,4,8 km s^{-1} (Smithsonian Astrophysical Observatory, Cambridge)
Lang, K.R. 1992, Astrophysical Data: Planets and Stars (Springer, New York)
Lanz, T. 1986, A&AS, 65, 195
Lindenblad, I. W. 1970, AJ, 75, 841
Lucy, L.B., & Sweeney, M.A. 1971, AJ, 76, 544
Mason, B.D. 1994, Ph.D. dissertation, Georgia State University
Mason, B.D. 1995, PASP, 107, 299

Mason, B.D., McAlister, H.A., Hartkopf, W.I., & Bagnuolo, Jr., W.G. 1993, AJ, 105, 220
McAlister, H.A., & Hartkopf, W.I. 1983, PASP, 95, 778
Muller, P. 1948, Ann. Obs. Strasbourg, 5, pt. 1
Muller, P. 1949, Ann. Obs. Strasbourg, 5, pt. 2
Pickering, E.C. 1879, Harvard Ann., 11, 105
Roberts, Jr., L.C., ten Brummelaar, T.A., Mason, B.D., Bagnuolo, Jr., W.G., & Turner, N.H. 1996 (in preparation)
Roberts D., Lehar, J., & Dreher, J. 1987, AJ, 93, 968
Strand, K.A. 1969, Pub. USNO, 18, pt. 5
Tokovinin, A.A., & Shatskii, N.I. 1995, SvAL, 1995, 21, 464
Turner, D.G., Lyons, R.W., & Bolton, C.T. 1986, Obs., 106, 13
Wickes, W.C. 1975, AJ, 80, 655
Wierzbinski, S. 1969, Wroclaw Obs. Contr., 16
Worley, C.E. 1969, AJ, 74, 764